

Spectral Function for the Anderson Model based on Nonequilibrium Perturbation Theory

Mami Hamasaki*

Department of Physics, Kyoto University, Kyoto 606-8502, Japan

(Dated: December 2, 2024)

Abstract

The spectral function based on the nonequilibrium perturbation theory up to the fourth-order is shown for the symmetric Anderson model and the characteristic of the Kondo resonance is investigated for nonequilibrium state caused by bias voltage. In accordance with the definition, the third-order and the fourth-order contributions to the retarded and advanced self-energies are derived from the nonequilibrium (real-time) perturbative expansion. In spectral function for equilibrium and electron correlation large enough, considerably high and sharp peaks rise at energy levels for the atomic limit. For bias voltage exceeding the Kondo temperature, the Kondo peak drops. The results suggest that the Kondo resonance can be destroyed owing to fluctuation of the Fermi level (the chemical potential) in nonequilibrium state.

PACS numbers: 72.15.Qm, 73.21.La, 71.27.+a

*Electronic address: hamasaki@scphys.kyoto-u.ac.jp

I. INTRODUCTION

The Kondo effect in electron transport through a quantum dot has been predicted theoretically at the end of 1980s, [1] and after a decade, this phenomenon has been observed. [2] The Kondo effect has been studied theoretically using the Anderson model and the predictions have been confirmed experimentally. In the Kondo regime, the conductance has been observed to reach the unitarity limit and the Kondo temperature estimated from observation is in excellent agreement with the expression derived using the Anderson model. [3] Furthermore, the Kondo effect in a quantum dot has been studied for nonequilibrium system where the bias voltage is applied. [4] Some theoretical work suggests that the Kondo peak splits into two peaks owing to bias voltage in the spectral density; [5, 6] however, it has not been established theoretically and has never been confirmed experimentally. Besides, in measurement of differential conductance, the Kondo peak splitting induced by source-drain voltage has not been observed for the spin-1/2 Kondo effect. Nevertheless, in different cases, the Kondo peak splitting of differential conductance takes place in the presence of applied voltage. [7, 8]

The nonequilibrium perturbation theory stands not only for equilibrium system but also for nonequilibrium system. The basic idea on the nonequilibrium perturbation theory based on the time-contour which starts and ends at $t = -\infty$ via $t = \infty$ has been proposed by Schwinger. [9] After that, the frame of the nonequilibrium perturbation theory has been built up using the nonequilibrium Green's functions introduced on the basis of the time-contour by Keldysh. [10] Since then, it has ever been developed in various field of physics. However, the system of the nonequilibrium perturbation theory and the method of perturbative expansion have been established incompletely; thus, there are various manners for perturbative expansion.

In condensed matter physics where electron correlation is effective strongly, the Yosida-Yamada theory [11]—perturbation theory for equilibrium based on the Fermi liquid theory [12] and confirmed to be valid for electron correlation from zero to infinity—is very successful. Hershfield *et al.* have extended the Yosida-Yamada theory to perturbation theory for nonequilibrium and have shown that the Kondo resonance comes to disappear for the bias voltage higher than the Kondo temperature in the spectral function based on the second-order perturbation theory for the Anderson model. [13] In study on nonequilibrium

perturbation theory, the perturbative expansion higher than the second-order has ever been left unsolved for more than ten years. Thus, the characteristic of the spectral function based on the perturbation theory higher than the second-order has not been clarified.

In the present work, the spectral function based on the nonequilibrium perturbation theory up to the fourth-order is shown for the Anderson model and the characteristic of the Kondo resonance is investigated for nonequilibrium state caused by applied dc voltage. In accordance with the definition, the third- and the fourth-order contributions to the retarded and advanced self-energies for the Anderson model are formulated from the nonequilibrium (real-time) perturbative expansion by extension of the Yosida-Yamada theory. The expressions for the third-order self-energy at equilibrium are in agreement with those derived from the Matubara imaginary-time perturbative expansion for equilibrium and analytical continuity by Zlatić *et al.* [14] For the fourth-order self-energy at equilibrium and the electron-hole symmetry, the asymptotic behavior at low energy agrees approximately with the exact results based on the Bethe ansatz method. [15] As numerical results, in spectral function based on the perturbation theory up to the fourth-order for equilibrium and electron correlation large enough, considerably high and sharp peaks rise at energy levels for the atomic limit. For bias voltage exceeding the Kondo temperature, the Kondo peak drops. The results suggest that the Kondo resonance can be destroyed because of fluctuation of the Fermi level (the chemical potential) in nonequilibrium state.

II. MODEL AND NONEQUILIBRIUM GREEN'S FUNCTIONS

We consider nonequilibrium stationary state. The system is described by the Anderson model connected to leads. The impurity with on-site energy E_0 and the Coulomb interaction U is connected to the left and right leads by the mixing matrix elements, v_L and v_R . The Anderson Hamiltonian is given by

$$\begin{aligned} \mathcal{H} = & E_0 \sum_{\sigma} \hat{n}_{d\sigma} + U(\hat{n}_{d\uparrow} - \langle \hat{n}_{d\uparrow} \rangle)(\hat{n}_{d\downarrow} - \langle \hat{n}_{d\downarrow} \rangle) \\ & - \sum_{\sigma} v_L (\hat{d}_{\sigma}^{\dagger} \hat{c}_{L\sigma} + \text{H.c.}) - \sum_{\sigma} v_R (\hat{d}_{\sigma}^{\dagger} \hat{c}_{R\sigma} + \text{H.c.}). \end{aligned} \quad (2.1)$$

\hat{d}^{\dagger} (\hat{d}) is creation (annihilation) operator for electron on the impurity, and \hat{c}_L^{\dagger} and \hat{c}_R^{\dagger} (\hat{c}_L and \hat{c}_R) are creation (annihilation) operators in the left and right leads, respectively. σ is

index for spin. The chemical potentials in the isolated left and right leads are μ_L and μ_R , respectively. Therefore, the applied voltage is defined by $eV \equiv \mu_L - \mu_R$.

Four nonequilibrium Green's functions are introduced by

$$G_{ij}^>(t_1, t_2) \equiv -i\langle \hat{d}_i(t_1)\hat{d}_j^\dagger(t_2) \rangle, \quad (2.2)$$

$$G_{ij}^<(t_1, t_2) \equiv i\langle \hat{d}_j^\dagger(t_2)\hat{d}_i(t_1) \rangle, \quad (2.3)$$

$$G_{ij}^r(t_1, t_2) \equiv -i\theta(t_1 - t_2)\langle \{\hat{d}_i(t_1), \hat{d}_j^\dagger(t_2)\} \rangle, \quad (2.4)$$

$$G_{ij}^a(t_1, t_2) \equiv i\theta(t_2 - t_1)\langle \{\hat{d}_i(t_1), \hat{d}_j^\dagger(t_2)\} \rangle, \quad (2.5)$$

where the angular brackets denote a thermal average in nonequilibrium and the curly brackets indicate an anticommutator. These nonequilibrium Green's functions are linearly related: $G_{ij}^a - G_{ij}^r = G_{ij}^< - G_{ij}^>$.

A thermal average in nonequilibrium can be obtained on the basis of the nonequilibrium perturbation theory. [16] Initially at $t = -\infty$, we assume that the impurity is disconnected from leads; the impurity and the isolated leads are in their respective thermal equilibrium. The mixing matrix elements are then turned on adiabatically. After that, the time evolution is expressed with a real-time contour, as illustrated in Fig. 1. The time integration in S matrix (S operator) is carried out along the path of the contour.

We consider that the band-width of left and right leads is large infinitely, so that the coupling functions, Γ_L , Γ_R can be taken to be independent of energy, E . On-site energy E_0 is set to cancel with the Hartree term, the first-order contribution to self-energy for electron correlation: $\Sigma_\sigma^{r(1)}(E) = \Sigma_\sigma^{a(1)}(E) = U \langle n_{-\sigma} \rangle$. Accordingly, the Fourier components of the noninteracting Green's functions can be written by

$$g^r(E) = \frac{1}{E + i\Gamma}, \quad (2.6)$$

$$g^a(E) = \frac{1}{E - i\Gamma}, \quad (2.7)$$

$$g^<(E) = g^r(E) [if_L(E)\Gamma_L + if_R(E)\Gamma_R] g^a(E), \quad (2.8)$$

$$g^>(E) = g^r(E) [i(1 - f_L(E))\Gamma_L + i(1 - f_R(E))\Gamma_R] g^a(E). \quad (2.9)$$

Here, $\Gamma = (\Gamma_L + \Gamma_R)/2$. f_L and f_R are the Fermi distribution functions in the isolated left and right leads, respectively.

III. SELF-ENERGY FOR ELECTRON CORRELATION

In accordance with the definition, the retarded and advanced self-energies are formulated from the nonequilibrium (real-time) perturbative expansion.

A. Second-Order Self-Energy

The second-order self-energy is written by:

$$\Sigma^{r(2)}(E) = U^2 \int_0^\infty dt_1 e^{iEt_1} \begin{bmatrix} g^\pm(t_1)g^>(t_1)g^<(-t_1) + g^<(t_1)g^\pm(t_1)g^>(-t_1) \\ + g^<(t_1)g^>(t_1)g^\pm(-t_1) \end{bmatrix}, \quad (3.1)$$

$$\Sigma^{a(2)}(E) = U^2 \int_{-\infty}^0 dt_1 e^{iEt_1} \begin{bmatrix} g^\pm(t_1)g^>(t_1)g^<(-t_1) + g^<(t_1)g^\pm(t_1)g^>(-t_1) \\ + g^<(t_1)g^>(t_1)g^\pm(-t_1) \end{bmatrix}. \quad (3.2)$$

Here $g^\pm(t) = g^r(t) + g^a(t)$, that is, $g^+(t) = g^r(t)$, for $t \geq 0$ and $g^-(t) = g^a(t)$, for $t < 0$. $g^r(t)$, $g^a(t)$, $g^<(t)$, and $g^>(t)$ are the inverse Fourier components of Eqs.(2.6)-(2.9). Figure 2 indicates the diagram for the second-order self-energy. In the symmetric equilibrium case, the asymptotic behavior at zero temperature and low energy is expressed by

$$\Sigma^{r(2)}(E) \simeq -\Gamma \left(3 - \frac{\pi^2}{4} \right) \left(\frac{U}{\pi\Gamma} \right)^2 \frac{E}{\Gamma} - i\frac{\Gamma}{2} \left(\frac{U}{\pi\Gamma} \right)^2 \left(\frac{E}{\Gamma} \right)^2, \quad (3.3)$$

the exact results based on the Bethe ansatz method. [11, 15]

B. Third-Order Self-Energy

The third-order contribution to the self-energy is shown. The terms corresponding to the diagram denoted in Fig. 3(a) are expressed by

$$\begin{aligned} \Sigma_{pp}^{r(3)}(E) = U^3 \int_0^\infty dt_1 \int_{-\infty}^\infty dt_2 e^{iEt_1} & \begin{bmatrix} g^<(-t_1)g^>(t_1 - t_2)g^>(t_1 - t_2) \\ -g^>(-t_1)g^<(t_1 - t_2)g^<(t_1 - t_2) \end{bmatrix} \\ & \times \begin{bmatrix} g^\pm(t_2)g^>(t_2) + g^<(t_2)g^\pm(t_2) \end{bmatrix}, \end{aligned} \quad (3.4)$$

$$\Sigma_{pp}^{a(3)}(E) = U^3 \int_{-\infty}^0 dt_1 \int_{-\infty}^{\infty} dt_2 e^{iEt_1} \begin{bmatrix} g^>(-t_1)g^<(t_1-t_2)g^<(t_1-t_2) \\ -g^<(-t_1)g^>(t_1-t_2)g^>(t_1-t_2) \end{bmatrix} \times \begin{bmatrix} g^{\pm}(t_2)g^>(t_2) + g^<(t_2)g^{\pm}(t_2) \end{bmatrix}. \quad (3.5)$$

Figure 3(b) illustrates the diagram for the following terms:

$$\Sigma_{ph}^{r(3)}(E) = U^3 \int_0^{\infty} dt_1 \int_{-\infty}^{\infty} dt_2 e^{iEt_1} \begin{bmatrix} g^>(t_1)g^>(t_1-t_2)g^<(t_2-t_1) \\ -g^<(t_1)g^<(t_1-t_2)g^>(t_2-t_1) \end{bmatrix} \times \begin{bmatrix} g^{\pm}(t_2)g^<(-t_2) + g^<(t_2)g^{\pm}(-t_2) \end{bmatrix}, \quad (3.6)$$

$$\Sigma_{ph}^{a(3)}(E) = U^3 \int_{-\infty}^0 dt_1 \int_{-\infty}^{\infty} dt_2 e^{iEt_1} \begin{bmatrix} g^<(t_1)g^<(t_1-t_2)g^>(t_2-t_1) \\ -g^>(t_1)g^>(t_1-t_2)g^<(t_2-t_1) \end{bmatrix} \times \begin{bmatrix} g^{\pm}(t_2)g^<(-t_2) + g^<(t_2)g^{\pm}(-t_2) \end{bmatrix}. \quad (3.7)$$

Equations (3.4)-(3.7) at equilibrium agree with those derived from the Matubara imaginary-time perturbative expansion for equilibrium and analytical continuity. [14]

C. Fourth-Order Self-Energy

The twelve kinds of terms for the proper fourth-order self-energy can be divided into four groups each comprised of three kinds of terms. The four groups correspond to the diagrams denoted in Figs. 4 (a)-(c), Figs. 4 (d)-(f), Figs. 4 (g)-(i), and Figs. 4 (j)-(l), respectively. The terms for the diagrams illustrated in Figs. 4(a) and 4(b) are equivalent except for the spin indices and expressed by

$$\Sigma_{a,b}^{r(4)}(E) = U^4 \int_0^{\infty} dt_1 \int_{-\infty}^{\infty} dt_2 \int_{-\infty}^{\infty} dt_3 e^{iEt_1} \begin{bmatrix} g^<(t_1)g^<(t_1-t_2-t_3)g^>(-t_1+t_2+t_3) \\ -g^>(t_1)g^>(t_1-t_2-t_3)g^<(-t_1+t_2+t_3) \end{bmatrix} \times \begin{bmatrix} g^{\pm}(t_2)g^<(-t_2) + g^<(t_2)g^{\pm}(-t_2) \end{bmatrix} \begin{bmatrix} g^{\pm}(t_3)g^<(-t_3) + g^<(t_3)g^{\pm}(-t_3) \end{bmatrix}, \quad (3.8)$$

$$\begin{aligned}
\Sigma_{a,b}^{a(4)}(E) &= U^4 \int_{-\infty}^0 dt_1 \int_{-\infty}^{\infty} dt_2 \int_{-\infty}^{\infty} dt_3 e^{iEt_1} \begin{bmatrix} g^>(t_1)g^>(t_1-t_2-t_3)g^<(-t_1+t_2+t_3) \\ -g^<(t_1)g^<(t_1-t_2-t_3)g^>(-t_1+t_2+t_3) \end{bmatrix} \\
&\times \begin{bmatrix} g^{\pm}(t_2)g^<(-t_2) + g^<(t_2)g^{\pm}(-t_2) \\ g^{\pm}(t_3)g^<(-t_3) + g^<(t_3)g^{\pm}(-t_3) \end{bmatrix}. \tag{3.9}
\end{aligned}$$

Additionally, Figure 4(c) indicates the diagram for the following terms:

$$\begin{aligned}
\Sigma_c^{r(4)}(E) &= U^4 \int_0^{\infty} dt_1 \int_{-\infty}^{\infty} dt_2 \int_{-\infty}^{\infty} dt_3 e^{iEt_1} \begin{bmatrix} g^>(-t_1)g^<(t_1-t_2-t_3)g^<(t_1-t_2-t_3) \\ -g^<(-t_1)g^>(t_1-t_2-t_3)g^>(t_1-t_2-t_3) \end{bmatrix} \\
&\times \begin{bmatrix} g^{\pm}(t_2)g^>(t_2) + g^<(t_2)g^{\pm}(t_2) \\ g^{\pm}(t_3)g^>(t_3) + g^<(t_3)g^{\pm}(t_3) \end{bmatrix}, \tag{3.10}
\end{aligned}$$

$$\begin{aligned}
\Sigma_c^{a(4)}(E) &= U^4 \int_{-\infty}^0 dt_1 \int_{-\infty}^{\infty} dt_2 \int_{-\infty}^{\infty} dt_3 e^{iEt_1} \begin{bmatrix} g^<(-t_1)g^>(t_1-t_2-t_3)g^>(t_1-t_2-t_3) \\ -g^>(-t_1)g^<(t_1-t_2-t_3)g^<(t_1-t_2-t_3) \end{bmatrix} \\
&\times \begin{bmatrix} g^{\pm}(t_2)g^>(t_2) + g^<(t_2)g^{\pm}(t_2) \\ g^{\pm}(t_3)g^>(t_3) + g^<(t_3)g^{\pm}(t_3) \end{bmatrix}. \tag{3.11}
\end{aligned}$$

Next, the terms brought from diagram in Fig. 4(d) are expressed by

$$\begin{aligned}
\Sigma_d^{r(4)}(E) &= U^4 \int_0^{\infty} dt_1 \int_{-\infty}^{\infty} dt_2 \int_{-\infty}^{\infty} dt_3 e^{iEt_1} \begin{bmatrix} g^>(t_1-t_3)g^>(t_1-t_2)g^<(t_2-t_1) \\ -g^<(t_1-t_3)g^<(t_1-t_2)g^>(t_2-t_1) \end{bmatrix} \\
&\times g^{\pm}(t_2) \text{sgn}(t_3) \begin{bmatrix} g^>(-t_2+t_3)g^>(t_3)g^<(-t_3) - g^<(-t_2+t_3)g^<(t_3)g^>(-t_3) \end{bmatrix}, \tag{3.12}
\end{aligned}$$

$$\begin{aligned}
\Sigma_d^{a(4)}(E) &= U^4 \int_{-\infty}^0 dt_1 \int_{-\infty}^{\infty} dt_2 \int_{-\infty}^{\infty} dt_3 e^{iEt_1} \begin{bmatrix} g^<(t_1-t_3)g^<(t_1-t_2)g^>(t_2-t_1) \\ -g^>(t_1-t_3)g^>(t_1-t_2)g^<(t_2-t_1) \end{bmatrix} \\
&\times g^{\pm}(t_2) \text{sgn}(t_3) \begin{bmatrix} g^>(-t_2+t_3)g^>(t_3)g^<(-t_3) - g^<(-t_2+t_3)g^<(t_3)g^>(-t_3) \end{bmatrix}. \tag{3.13}
\end{aligned}$$

The terms for diagram in Fig. 4(e) are written by

$$\begin{aligned}
\Sigma_e^{r(4)}(E) &= U^4 \int_0^{\infty} dt_1 \int_{-\infty}^{\infty} dt_2 \int_{-\infty}^{\infty} dt_3 e^{iEt_1} \begin{bmatrix} g^>(t_1-t_2)g^>(t_1-t_2)g^<(t_3-t_1) \\ -g^<(t_1-t_2)g^<(t_1-t_2)g^>(t_3-t_1) \end{bmatrix} \\
&\times g^{\pm}(t_2) \text{sgn}(t_3) \begin{bmatrix} g^>(t_2-t_3)g^>(-t_3)g^<(t_3) - g^<(t_2-t_3)g^<(-t_3)g^>(t_3) \end{bmatrix}, \tag{3.14}
\end{aligned}$$

$$\begin{aligned} \Sigma_e^{a(4)}(E) &= U^4 \int_{-\infty}^0 dt_1 \int_{-\infty}^{\infty} dt_2 \int_{-\infty}^{\infty} dt_3 e^{iEt_1} \begin{bmatrix} g^<(t_1 - t_2)g^<(t_1 - t_2)g^>(t_3 - t_1) \\ -g^>(t_1 - t_2)g^>(t_1 - t_2)g^<(t_3 - t_1) \end{bmatrix} \\ &\times g^{\pm}(t_2) \operatorname{sgn}(t_3) \begin{bmatrix} g^>(t_2 - t_3)g^>(-t_3)g^<(t_3) - g^<(t_2 - t_3)g^<(-t_3)g^>(t_3) \end{bmatrix}. \end{aligned} \quad (3.15)$$

In addition, Figure 4(f) denotes the diagram for the following terms:

$$\begin{aligned} \Sigma_f^{r(4)}(E) &= U^4 \int_0^{\infty} dt_1 \int_{-\infty}^{\infty} dt_2 \int_{-\infty}^{\infty} dt_3 e^{iEt_1} \begin{bmatrix} g^>(t_1 - t_3)g^>(t_1 - t_2)g^<(t_2 - t_1) \\ -g^<(t_1 - t_3)g^<(t_1 - t_2)g^>(t_2 - t_1) \end{bmatrix} \\ &\times g^{\pm}(-t_2) \operatorname{sgn}(t_3) \begin{bmatrix} g^<(t_3)g^<(t_3)g^>(t_2 - t_3) - g^>(t_3)g^>(t_3)g^<(t_2 - t_3) \end{bmatrix}, \end{aligned} \quad (3.16)$$

$$\begin{aligned} \Sigma_f^{a(4)}(E) &= U^4 \int_{-\infty}^0 dt_1 \int_{-\infty}^{\infty} dt_2 \int_{-\infty}^{\infty} dt_3 e^{iEt_1} \begin{bmatrix} g^<(t_1 - t_3)g^<(t_1 - t_2)g^>(t_2 - t_1) \\ -g^>(t_1 - t_3)g^>(t_1 - t_2)g^<(t_2 - t_1) \end{bmatrix} \\ &\times g^{\pm}(-t_2) \operatorname{sgn}(t_3) \begin{bmatrix} g^<(t_3)g^<(t_3)g^>(t_2 - t_3) - g^>(t_3)g^>(t_3)g^<(t_2 - t_3) \end{bmatrix}. \end{aligned} \quad (3.17)$$

Next, the terms formulated from diagram illustrated in Fig. 4(g) are expressed by

$$\begin{aligned} \Sigma_g^{r(4)}(E) &= U^4 \int_0^{\infty} dt_1 \int_{-\infty}^{\infty} dt_2 \int_{-\infty}^{\infty} dt_3 e^{iEt_1} \begin{bmatrix} g^>(t_1)g^>(t_1 - t_2 - t_3)g^<(t_2 - t_1) \\ -g^<(t_1)g^<(t_1 - t_2 - t_3)g^>(t_2 - t_1) \end{bmatrix} \\ &\times g^{\pm}(-t_2) \operatorname{sgn}(t_3) \begin{bmatrix} g^>(t_2 + t_3)g^>(t_3)g^<(-t_3) - g^<(t_2 + t_3)g^<(t_3)g^>(-t_3) \end{bmatrix}, \end{aligned} \quad (3.18)$$

$$\begin{aligned} \Sigma_g^{a(4)}(E) &= U^4 \int_{-\infty}^0 dt_1 \int_{-\infty}^{\infty} dt_2 \int_{-\infty}^{\infty} dt_3 e^{iEt_1} \begin{bmatrix} g^<(t_1)g^<(t_1 - t_2 - t_3)g^>(t_2 - t_1) \\ -g^>(t_1)g^>(t_1 - t_2 - t_3)g^<(t_2 - t_1) \end{bmatrix} \\ &\times g^{\pm}(-t_2) \operatorname{sgn}(t_3) \begin{bmatrix} g^>(t_2 + t_3)g^>(t_3)g^<(-t_3) - g^<(t_2 + t_3)g^<(t_3)g^>(-t_3) \end{bmatrix}. \end{aligned} \quad (3.19)$$

Figure 4(h) illustrates the diagram for the following terms:

$$\begin{aligned} \Sigma_h^{r(4)}(E) &= U^4 \int_0^{\infty} dt_1 \int_{-\infty}^{\infty} dt_2 \int_{-\infty}^{\infty} dt_3 e^{iEt_1} \begin{bmatrix} g^<(t_1)g^<(t_1 - t_2 - t_3)g^>(t_2 - t_1) \\ -g^>(t_1)g^>(t_1 - t_2 - t_3)g^<(t_2 - t_1) \end{bmatrix} \\ &\times g^{\pm}(t_2) \operatorname{sgn}(t_3) \begin{bmatrix} g^>(t_3)g^>(t_3)g^<(-t_2 - t_3) - g^<(t_3)g^<(t_3)g^>(-t_2 - t_3) \end{bmatrix}, \end{aligned} \quad (3.20)$$

$$\begin{aligned} \Sigma_h^{a(4)}(E) &= U^4 \int_{-\infty}^0 dt_1 \int_{-\infty}^{\infty} dt_2 \int_{-\infty}^{\infty} dt_3 e^{iEt_1} \begin{bmatrix} g^>(t_1)g^>(t_1 - t_2 - t_3)g^<(t_2 - t_1) \\ -g^<(t_1)g^<(t_1 - t_2 - t_3)g^>(t_2 - t_1) \end{bmatrix} \\ &\times g^{\pm}(t_2) \operatorname{sgn}(t_3) \begin{bmatrix} g^>(t_3)g^>(t_3)g^<(-t_2 - t_3) - g^<(t_3)g^<(t_3)g^>(-t_2 - t_3) \end{bmatrix}. \end{aligned} \quad (3.21)$$

Besides, the terms formulated from the diagram in Fig. 4(i) are written by

$$\begin{aligned} \Sigma_i^{r(4)}(E) &= U^4 \int_0^{\infty} dt_1 \int_{-\infty}^{\infty} dt_2 \int_{-\infty}^{\infty} dt_3 e^{iEt_1} \begin{bmatrix} g^>(-t_1)g^<(t_1 - t_2 - t_3)g^<(t_1 - t_2) \\ -g^<(-t_1)g^>(t_1 - t_2 - t_3)g^>(t_1 - t_2) \end{bmatrix} \\ &\times g^{\pm}(t_2) \operatorname{sgn}(t_3) \begin{bmatrix} g^>(t_2 + t_3)g^>(t_3)g^<(-t_3) - g^<(t_2 + t_3)g^<(t_3)g^>(-t_3) \end{bmatrix}, \end{aligned} \quad (3.22)$$

$$\begin{aligned} \Sigma_i^{a(4)}(E) &= U^4 \int_{-\infty}^0 dt_1 \int_{-\infty}^{\infty} dt_2 \int_{-\infty}^{\infty} dt_3 e^{iEt_1} \begin{bmatrix} g^<(-t_1)g^>(t_1 - t_2 - t_3)g^>(t_1 - t_2) \\ -g^>(-t_1)g^<(t_1 - t_2 - t_3)g^<(t_1 - t_2) \end{bmatrix} \\ &\times g^{\pm}(t_2) \operatorname{sgn}(t_3) \begin{bmatrix} g^>(t_2 + t_3)g^>(t_3)g^<(-t_3) - g^<(t_2 + t_3)g^<(t_3)g^>(-t_3) \end{bmatrix}. \end{aligned} \quad (3.23)$$

Next, the terms for diagrams denoted in Figs. 4 (j) and 4(k) are equivalent except for the spin indices and written by

$$\begin{aligned} \Sigma_{j,k}^{r(4)}(E) &= U^4 \int_0^{\infty} dt_1 \int_{-\infty}^{\infty} dt_2 \int_{-\infty}^{\infty} dt_3 e^{iEt_1} \begin{bmatrix} g^>(t_1)g^<(-t_1)g^>(t_1 - t_2 - t_3) \\ -g^<(t_1)g^>(-t_1)g^<(t_1 - t_2 - t_3) \end{bmatrix} \\ &\times g^{\pm}(t_2) \begin{bmatrix} g^{\pm}(t_3)g^>(t_3)g^<(-t_3) + g^<(t_3)g^{\pm}(t_3)g^>(-t_3) \\ +g^<(t_3)g^>(t_3)g^{\pm}(-t_3) \end{bmatrix}, \end{aligned} \quad (3.24)$$

$$\begin{aligned} \Sigma_{j,k}^{a(4)}(E) &= U^4 \int_{-\infty}^0 dt_1 \int_{-\infty}^{\infty} dt_2 \int_{-\infty}^{\infty} dt_3 e^{iEt_1} \begin{bmatrix} g^<(t_1)g^>(-t_1)g^<(t_1 - t_2 - t_3) \\ -g^>(t_1)g^<(-t_1)g^>(t_1 - t_2 - t_3) \end{bmatrix} \\ &\times g^{\pm}(t_2) \begin{bmatrix} g^{\pm}(t_3)g^>(t_3)g^<(-t_3) + g^<(t_3)g^{\pm}(t_3)g^>(-t_3) \\ +g^<(t_3)g^>(t_3)g^{\pm}(-t_3) \end{bmatrix}. \end{aligned} \quad (3.25)$$

In addition, the terms for diagram illustrated in Fig. 4(l) are expressed by

$$\begin{aligned} \Sigma_l^{r(4)}(E) = U^4 \int_0^\infty dt_1 \int_{-\infty}^\infty dt_2 \int_{-\infty}^\infty dt_3 e^{iEt_1} & \left[\begin{array}{l} g^>(t_1)g^>(t_1)g^<(-t_1+t_2+t_3) \\ -g^<(t_1)g^<(t_1)g^>(-t_1+t_2+t_3) \end{array} \right] \\ & \times g^\pm(-t_2) \left[\begin{array}{l} g^\pm(-t_3)g^>(-t_3)g^<(t_3) + g^<(-t_3)g^\pm(-t_3)g^>(t_3) \\ +g^<(-t_3)g^>(-t_3)g^\pm(t_3) \end{array} \right], \end{aligned} \quad (3.26)$$

$$\begin{aligned} \Sigma_l^{a(4)}(E) = U^4 \int_{-\infty}^0 dt_1 \int_{-\infty}^\infty dt_2 \int_{-\infty}^\infty dt_3 e^{iEt_1} & \left[\begin{array}{l} g^<(t_1)g^<(t_1)g^>(-t_1+t_2+t_3) \\ -g^>(t_1)g^>(t_1)g^<(-t_1+t_2+t_3) \end{array} \right] \\ & \times g^\pm(-t_2) \left[\begin{array}{l} g^\pm(-t_3)g^>(-t_3)g^<(t_3) + g^<(-t_3)g^\pm(-t_3)g^>(t_3) \\ +g^<(-t_3)g^>(-t_3)g^\pm(t_3) \end{array} \right]. \end{aligned} \quad (3.27)$$

For symmetric Anderson model at equilibrium, the asymptotic behavior at low energy is approximately in agreement with those based on the Bethe ansatz method [15]:

$$\Sigma^{r(4)}(E) \simeq -\Gamma \left(105 - \frac{45\pi^2}{4} + \frac{\pi^4}{16} \right) \left(\frac{U}{\pi\Gamma} \right)^4 \frac{E}{\Gamma} - i \frac{\Gamma}{2} (30 - 3\pi^2) \left(\frac{U}{\pi\Gamma} \right)^4 \left(\frac{E}{\Gamma} \right)^2. \quad (3.28)$$

IV. NUMERICAL RESULTS AND DISCUSSION

A. Self-Energy

For the symmetric Anderson model, the third-order self-energy, Eqs. (3. 4)-(3. 7) cancel respectively: $\Sigma_{ph}^{r(3)}(E) = -\Sigma_{pp}^{r(3)}(E)$, $\Sigma_{ph}^{a(3)}(E) = -\Sigma_{pp}^{a(3)}(E)$ not only at equilibrium but also at nonequilibrium where the voltage is applied without breaking electron-hole symmetry: $\mu_L = eV/2$ and $\mu_R = -eV/2$. As a consequence, the third-order contribution to self-energy vanish in the symmetric case.

For the fourth-order self-energy, three terms each comprised in the four groups contribute equivalently to self-energy in the symmetric case. The second-order and the fourth-order contributions to self-energy for zero temperature are shown in Figs. 5(a) and 5(b) and Figs. 6(a) and 6(b), respectively. Equation (3.3) represent the curves around energy of zero for equilibrium denoted by solid line in Figs. 5(a) and 5(b), respectively, and Equation (3.28) represent those approximately in Figs. 6(a) and 6(b), respectively. The fourth-order

contribution oscillates more than the second-order. When the voltage, eV/Γ exceeds ~ 2.0 , the behavior changes distinctly and comes to present striking contrasts to that for the second-order contribution. Especially, the curves for the imaginary part of the fourth-order contribution rise up considerably high with maximum at energy of zero at high voltage. On the other hand, for the second-order contribution, very deep valley appears with minimum at energy of zero—it is quite the contrary.

B. Spectral Function

The spectral function with the second-order self-energy is as generally known. It is plotted for $U/\Gamma = 10.0$ and zero temperature in Fig. 7. For equilibrium, the Kondo peak at energy of zero is very sharp and the two-side broad peaks appear at $E \simeq \pm U/2$. As eV becomes higher in comparison with the Kondo temperature, $k_B T_K$ [17], the Kondo peak for $eV/\Gamma = 1.0$ becomes gradually lower, but survives barely. For $eV/\Gamma = 2.0$, it lowers and finally, vanishes, while the two-side broad peaks rise at $E \simeq \pm U/2$.

Figure 8(a) shows the spectral function with the self-energy up to the fourth-order for equilibrium and zero temperature. With strengthening U , two-side narrow peaks come to occur in the vicinity of $E = \pm U/2$ in addition to the Kondo peak. At U large enough, the Kondo peak become very acute and two-side narrow peaks rise considerably higher and sharpen; the energy levels for the atomic limit are distinctly produced. Even in such a case, the Kondo peak at energy of zero reaches the unitarity limit and the charge, $\langle n \rangle$ corresponds to 1/2. Thereby, the Friedel sum rule is correctly satisfied: [18]

$$\rho(E_f) = \sin^2(\pi\langle n \rangle)/\pi\Gamma, \quad (4.1)$$

where $\rho(E_f)$ is the local density of states at the Fermi energy. However, since the curve for imaginary part of the fourth-order contribution is positive partially, as shown in Fig. 6(b), the spectral function can not be expressed with only the self-energy up to the fourth-order when U becomes too large. The higher-order contribution must be required in such cases. It is expected that only three sharp peaks at the energy levels for the atomic limit remain in the true spectral function involving all order perturbation terms.

Besides, the results for nonequilibrium and zero temperature are shown below. The expression for the Friedel sum rule, Eq. (4.1) does not stand for nonequilibrium, since the

charge can not be expressed with respect to the local density of states. However, the Kondo peak reaches the unitarity limit and $\langle n \rangle = 1/2$ in the symmetric and noninteracting case.

The spectral functions with the self-energy up to the fourth-order are plotted for $eV/\Gamma = 0.5$ and $eV/\Gamma = 1.0$ in Figs. 8(b) and 8(c), respectively. When U is strengthened and then, eV exceeds $k_B T_K$, the Kondo peak for $eV/\Gamma = 0.5$ drops but remains very small. Instead, the two-side narrow peaks grow to sharpen in the vicinity of $E = \pm U/2$. For $eV/\Gamma = 1.0$, the Kondo peak becomes broad and disappears for U large enough. The two-side peaks are generated small in the vicinity of $E = \pm U/2$. The Kondo resonance is quite broken owing to bias voltage. At $eV/\Gamma > \sim 2.0$, the Kondo peak does not lower even when eV is much larger than $k_B T_K$. The higher-order contribution to self-energy must be required to investigate the effect of electron correlation for high voltage.

In the present work, the effects of the electron correlation and of nonequilibrium are dealt with. It is concluded that the destruction of the Kondo resonance is due to the effect of nonequilibrium. For finite voltage, the impurity is in nonequilibrium state; in phenomenological words, the Fermi level (the chemical potential) fluctuates owing to nonequilibrium. Consequently, the Kondo peak becomes broad for $eV/\Gamma = 1.0$, as shown in Fig. 8(c), and the Kondo resonance at the Fermi level comes to be broken as bias voltage exceeds the Kondo temperature. These results suggest that the Kondo resonance at the Fermi level can be destroyed because of fluctuation of the Fermi level (the chemical potential) in nonequilibrium state generated by bias voltage. The physical picture of nonequilibrium state caused by bias voltage is generally known. [19] When the mixing between the impurity and the leads is large enough and the impurity is in nonequilibrium state, the chemical potential for the impurity is not fixed in real nonequilibrium state; the chemical potential fluctuates ranging approximately from μ_R to μ_L and the average of the chemical potential is within the range approximately from μ_R to μ_L . In nonequilibrium state, there are not two kinds of the chemical potentials induced by μ_L and μ_R , respectively. Hence, in nonequilibrium state, the Kondo peak does not split into two peaks at two kinds of the chemical potentials. Additionally, on the other hand, if the mixing between the impurity and the leads is very weak, then, the chemical potential for the impurity is shifted to the vicinity of μ_L or μ_R ; the impurity is in one equilibrium state of two kinds of equilibrium states. Accordingly, the Kondo peak is shifted to the vicinity of μ_L or μ_R . In such a case, the sense of the spectral function for the impurity has been lost.

Acknowledgments

The author would like to thank Professor K. Yamada and Dr. V. Zlatić for invaluable advice. The numerical calculations were performed at the Yukawa Institute Computer Facility. Additionally, the multiple integrals were executed using the computer subroutine, *MQFSRD* of NUMPAC.

- [1] T.-K. Ng and P. A. Lee, Phys. Rev. Lett. **61**, 1768 (1988); L. I. Glazman and M. E. Raikh, JETP Lett. **47**, 452 (1988).
- [2] D. Goldhaber-Gordon, H. Shtrikman, D. Mahalu, D. Abusch-Magder, U. Meirav, and M. A. Kastner, Nature (London) **391**, 156 (1998).
- [3] W. G. van der Wiel, S. De Franceschi, T. Fujisawa, J. M. Elzerman, S. Tarucha, and L. P. Kouwenhoven, Science **289**, 2105 (2000).
- [4] S. M. Cronenwett, T. H. Oosterkamp, and L. P. Kouwenhoven, Science **281**, 540 (1998).
- [5] Y. Meir, N. S. Wingreen, and P. A. Lee, Phys. Rev. Lett **70**, 2601 (1993).
- [6] T. Fujii and K. Ueda, Phys. Rev. B **68**, 155310 (2003).
- [7] S. De Franceschi, R. Hanson, W. G. van der Wiel, J. M. Elzerman, J. J. Wijpkema, T. Fujisawa, S. Tarucha, and L. P. Kouwenhoven, Phys. Rev. Lett. **89**, 156801 (2002).
- [8] J. Nygård, W. F. Koehl, N. Mason, L. DiCarlo, and C. M. Marcus, cond-mat/0410467.
- [9] J. Schwinger, J. Math. Phys. **2**, 407 (1961).
- [10] L. V. Keldysh, Sov. Phys. JETP **20**, 1018 (1965).
- [11] K. Yosida and K. Yamada, Prog. Theor. Phys. Suppl. **46**, 244 (1970); K. Yamada, Prog. Theor. Phys. **53**, 970 (1975); **55**, 1345 (1976).
- [12] P. Nozières, J. Low Temp. Phys. **17**, 31 (1974).
- [13] S. Hershfield, J. H. Davies and J. W. Wilkins, Phys. Rev. B **46**, 7046 (1992).
- [14] V. Zlatić, B. Horvatić, B. Dolički, S. Grabowski, P. Entel, and K.-D. Schotte, Phys. Rev. B **63**, 35104 (2000).
- [15] A. Okiji, *Fermi Surface Effects* edited by J. Kondo and A. Yoshimori (Springer, 1988).
- [16] C. Caroli, R. Combescot, P. Nozières and D. Saint-James, J. Phys. C **4**, 916 (1971).
- [17] V. Zlatić and B. Horvatić, Phys. Rev. B **28**, 6904 (1983).

[18] A. C. Hewson, *The Kondo Problem to Heavy Fermions* (Cambridge University Press, Cambridge, 1993). Figure 5.7 in this book shows the spectral density with only the 2nd-order self-energy; the caption for Fig. 5.7 is erroneous.

[19] For example, see S. Datta, *Electronic Transport In Mesoscopic Systems* (Cambridge University Press, Cambridge, 1995).

Fig. 1 The time-contour which starts and ends at $t = -\infty$.

Fig. 2 The diagram for the second-order self-energy. The solid line denotes the noninteracting Green's function and the dashed line indicates interaction.

Figs. 3 (a) (b) The two kinds of diagrams for the third-order self-energy.

Figs. 4 (a) (b) (c), Figs. 4 (d) (e) (f), Figs. 4 (g) (h) (i), Figs. 4 (j) (k) (l)
The twelve kinds of terms for the proper fourth-order self-energy divided into four groups.

Figs. 5 The second-order self-energy for the symmetric Anderson model at $U/\Gamma = 1.0$ and zero temperature. (a) the real part and (b) the imaginary part. Equilibrium (solid line), $eV/\Gamma = 1.0$ (thin solid line), and $eV/\Gamma = 2.0$ (dashed line).

Figs. 6 The fourth-order self-energy for the symmetric Anderson model at $U/\Gamma = 1.0$ and zero temperature. (a) the real part and (b) the imaginary part. Equilibrium (solid line), $eV/\Gamma = 1.0$ (thin solid line), and $eV/\Gamma = 2.0$ (dashed line).

Fig. 7 The spectral function with the second-order self-energy at $U/\Gamma = 10.0$ and zero-temperature for the symmetric Anderson model. Equilibrium (solid line), $eV/\Gamma = 1.0$ (thin solid line), and $eV/\Gamma = 2.0$ (dashed line).

Fig. 8(a) The spectral function with self-energy up to the fourth-order at equilibrium and zero-temperature for the symmetric Anderson model. $U/\Gamma = 3.5$ (dashed line), $U/\Gamma = 5.0$ (thin solid line), and $U/\Gamma = 6.0$ (solid line).

Fig. 8(b) The spectral function with self-energy up to the fourth-order at $eV/\Gamma = 0.5$ and zero-temperature for the symmetric Anderson model. $U/\Gamma = 3.5$ (dashed line), $U/\Gamma = 5.0$ (thin solid line), and $U/\Gamma = 6.0$ (solid line).

Fig. 8(c) The spectral function with self-energy up to the fourth-order at $eV/\Gamma = 1.0$ and zero-temperature for the symmetric Anderson model. $U/\Gamma = 3.5$ (dashed line), $U/\Gamma = 5.0$ (thin solid line), and $U/\Gamma = 6.0$ (solid line).

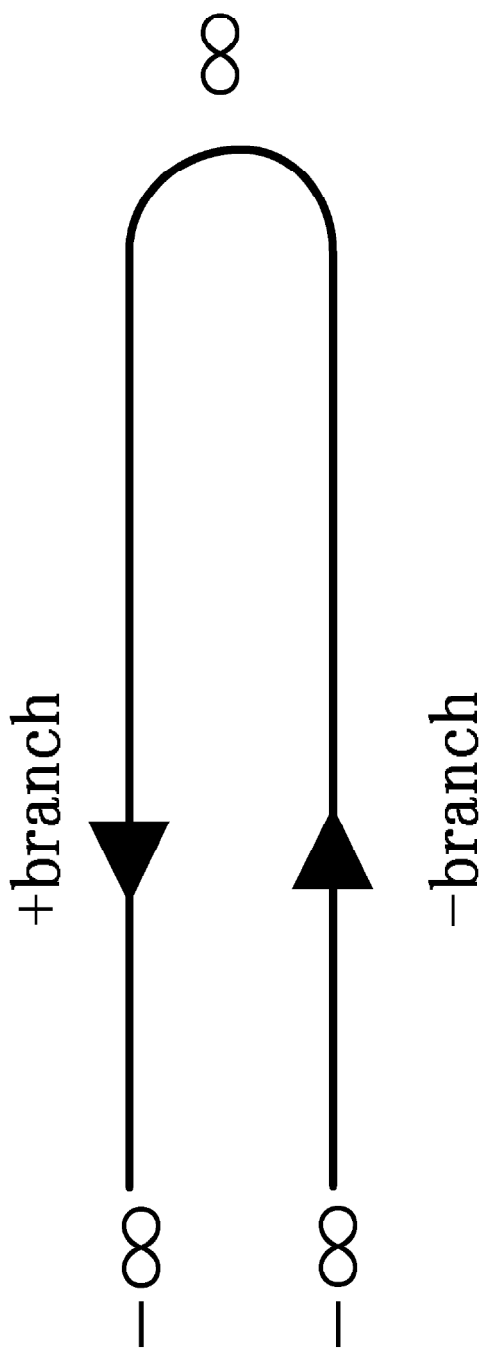


Fig. 1 Hamasaki

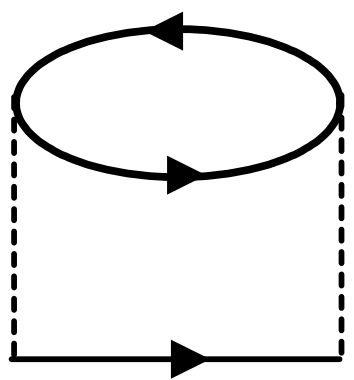


Fig.2 **Hamasaki**

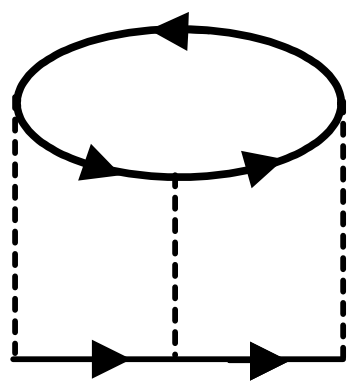


Fig.3(a) Hamasaki

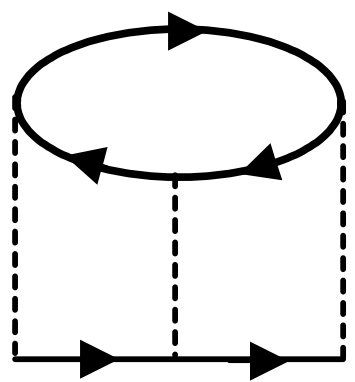


Fig.3(b) Hamasaki

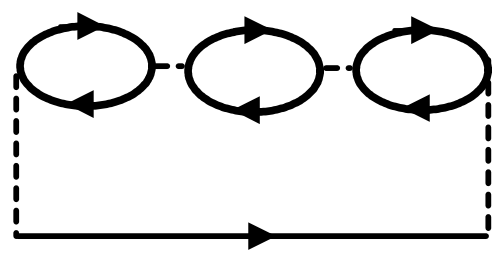


Fig.4(a) Hamasaki

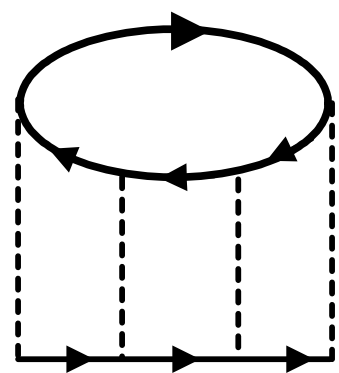


Fig.4(b) Hamasaki

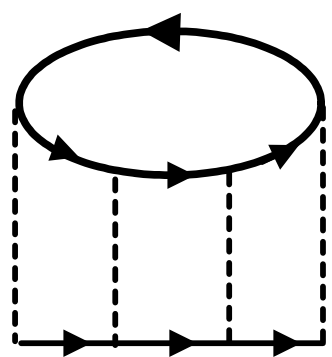


Fig.4(c) Hamasaki

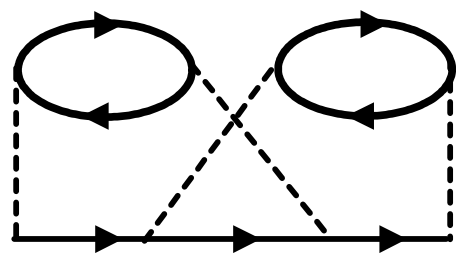


Fig.4(d) hamasaki

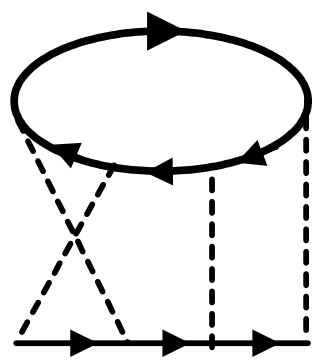


Fig.4(e) Hamasaki

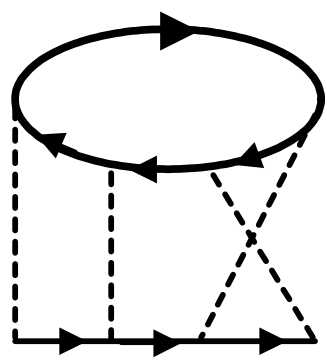


Fig.4(f) Hamasaki

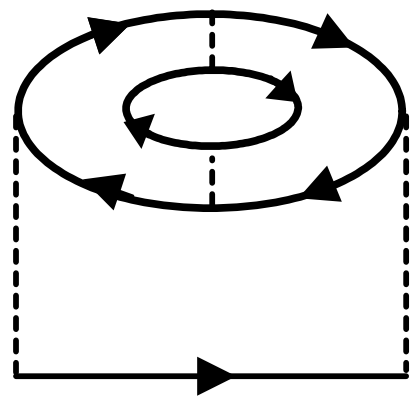


Fig.4(g) Hamasaki

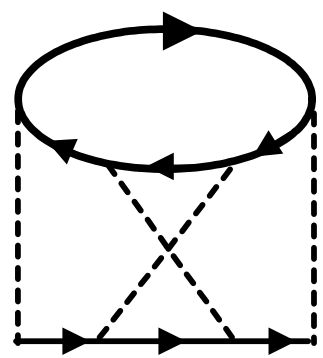


Fig.4(h) Hamasaki

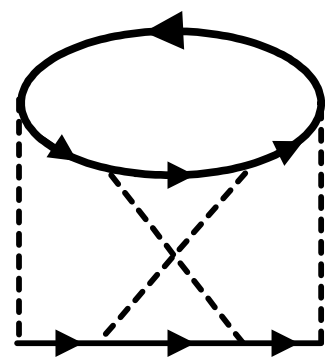


Fig.4(i) Hamasaki

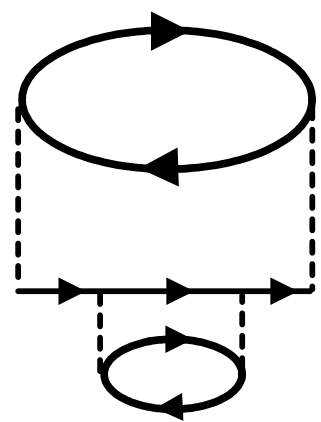


Fig.4(j) Hamasaki

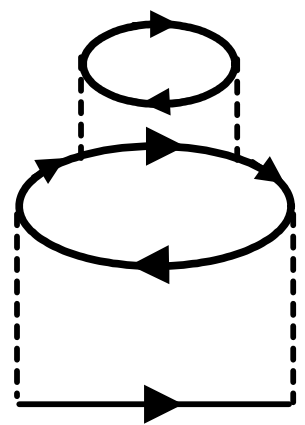


Fig.4(k) Hamasaki

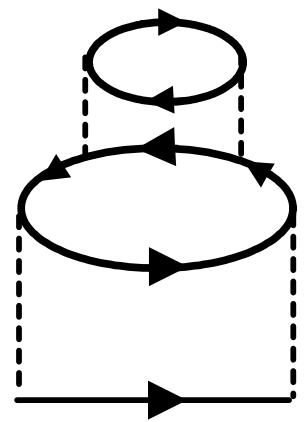


Fig.4(l) Hamasaki

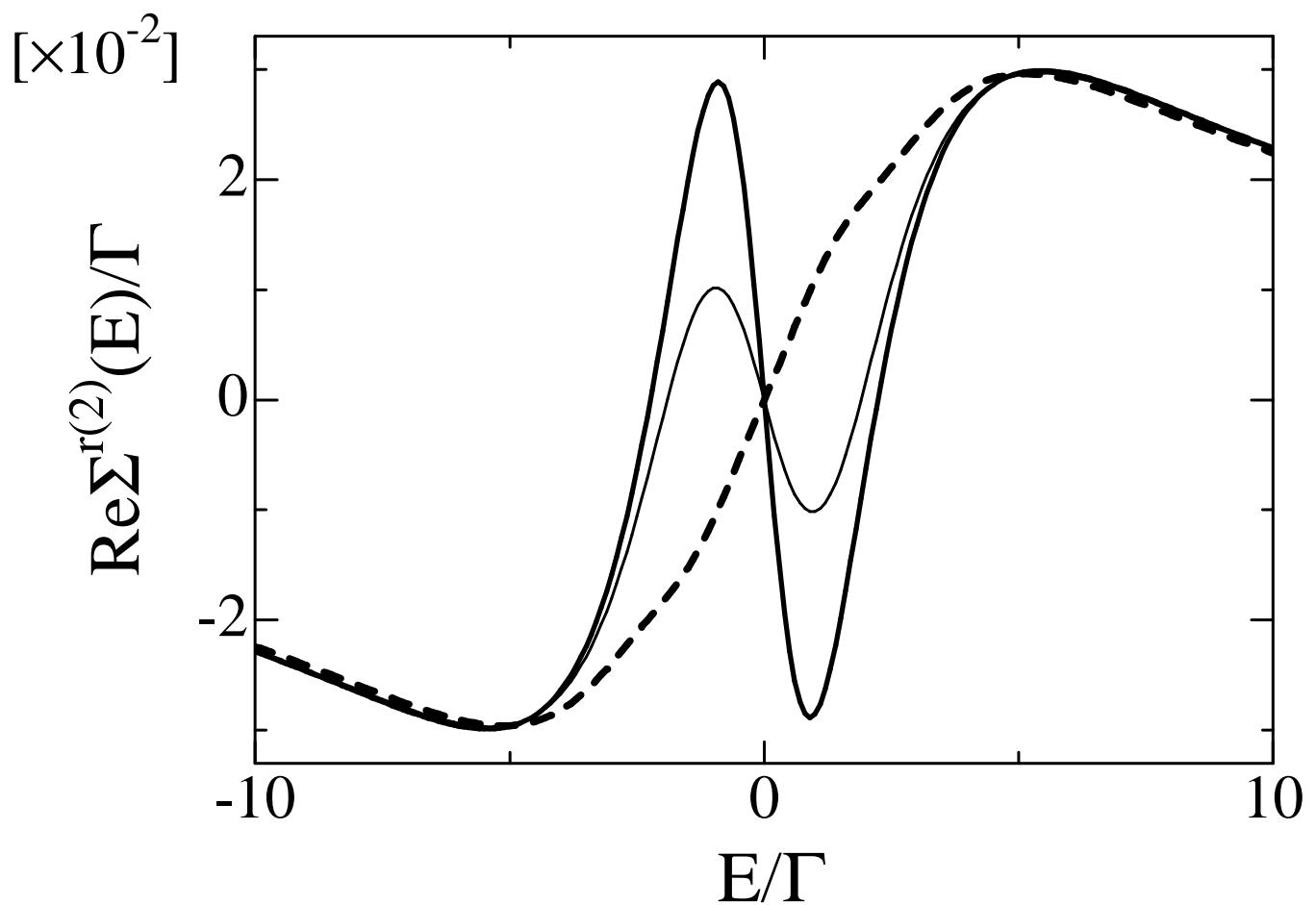


Fig.5(a) Hamasaki

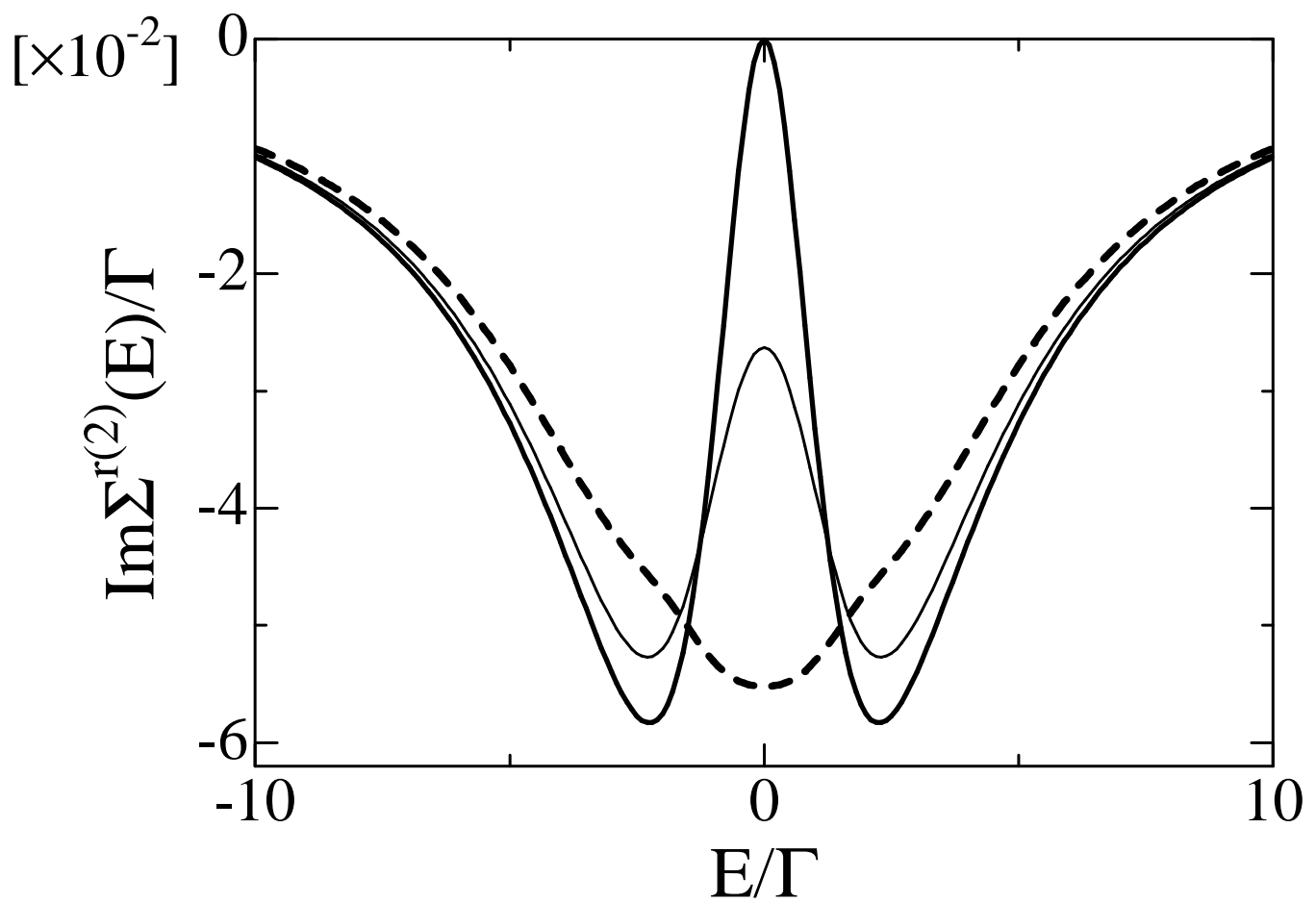


Fig.5(b) Hamasaki

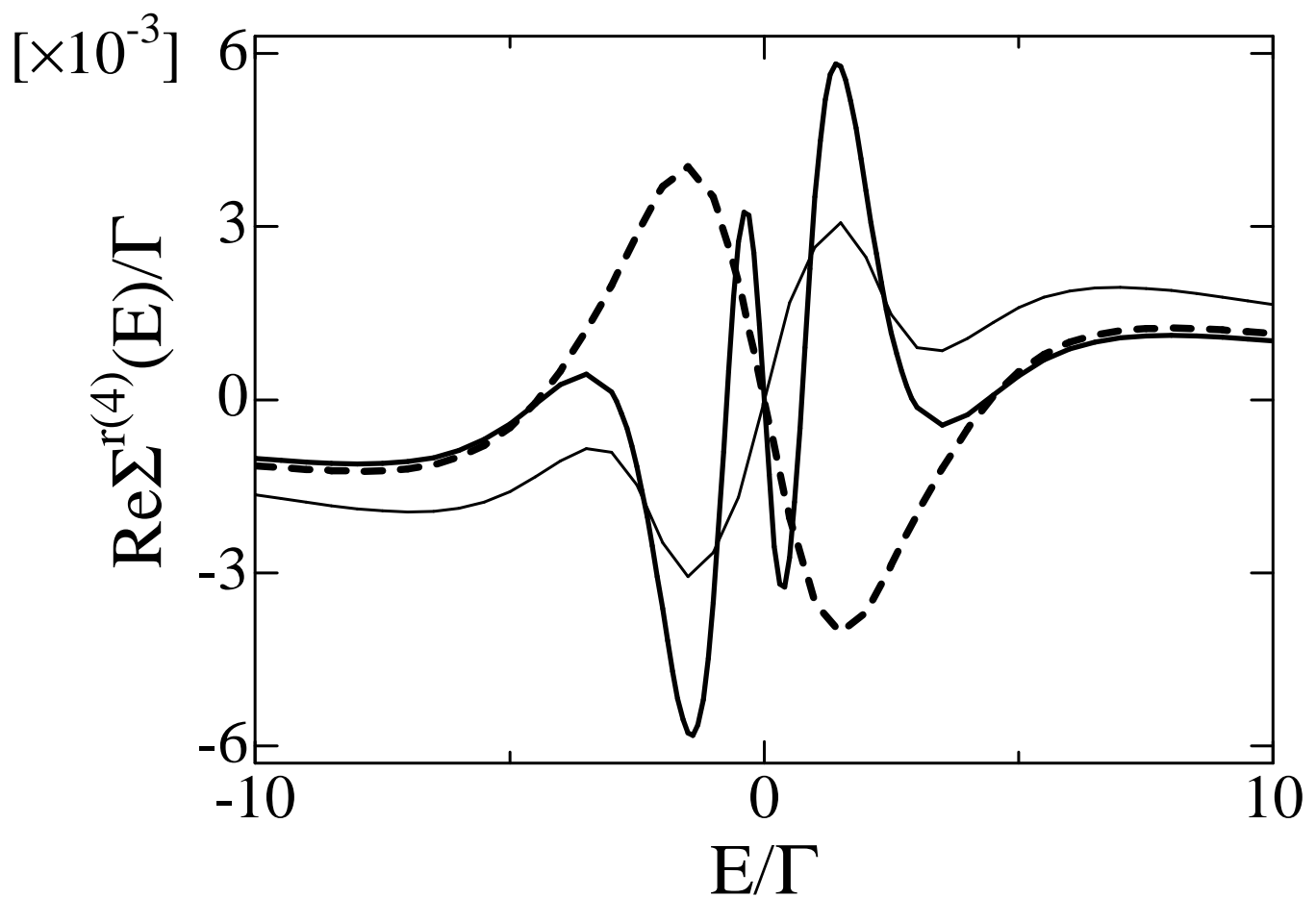


Fig.6(a) Hamasaki

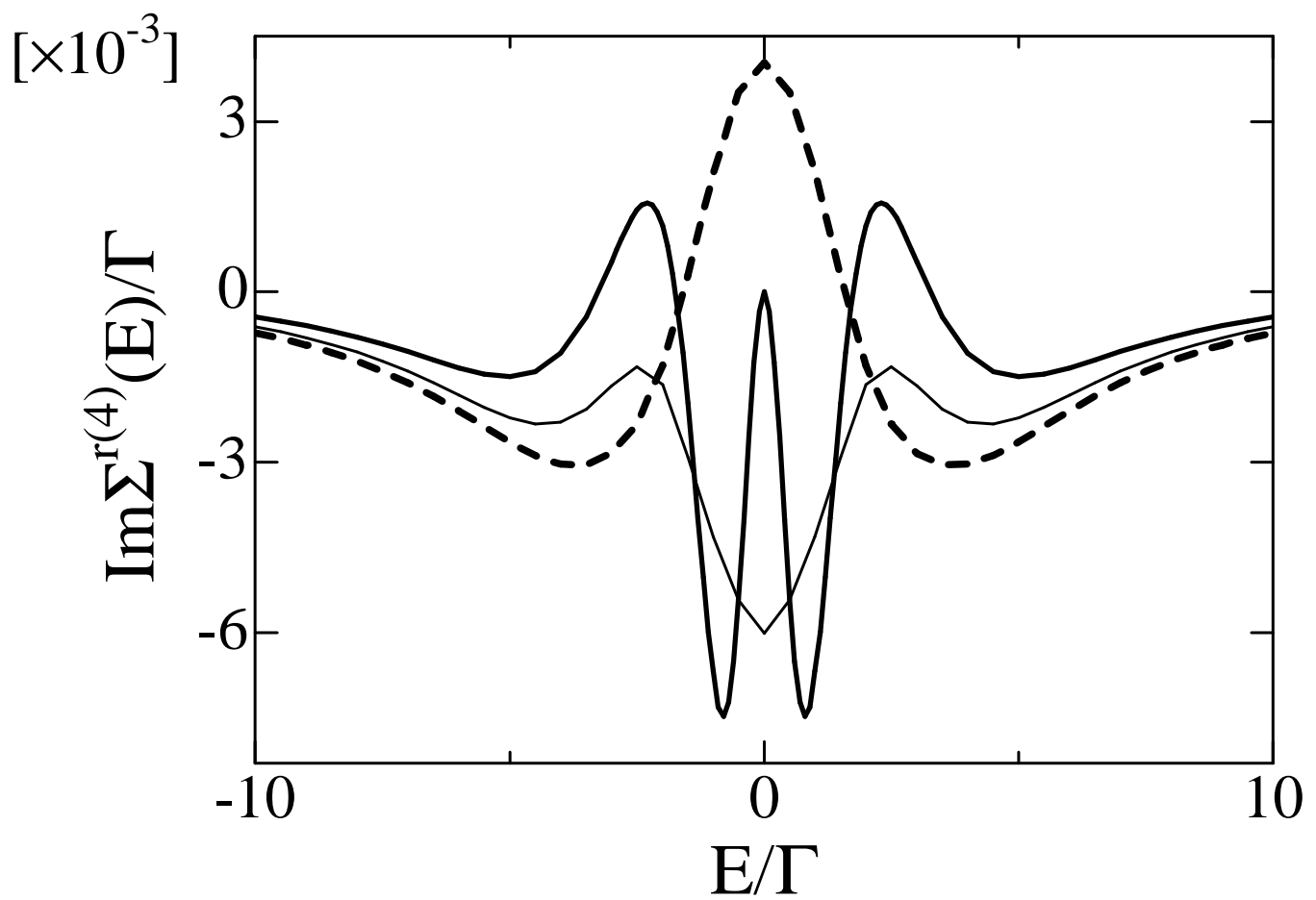


Fig.6(b) Hamasaki

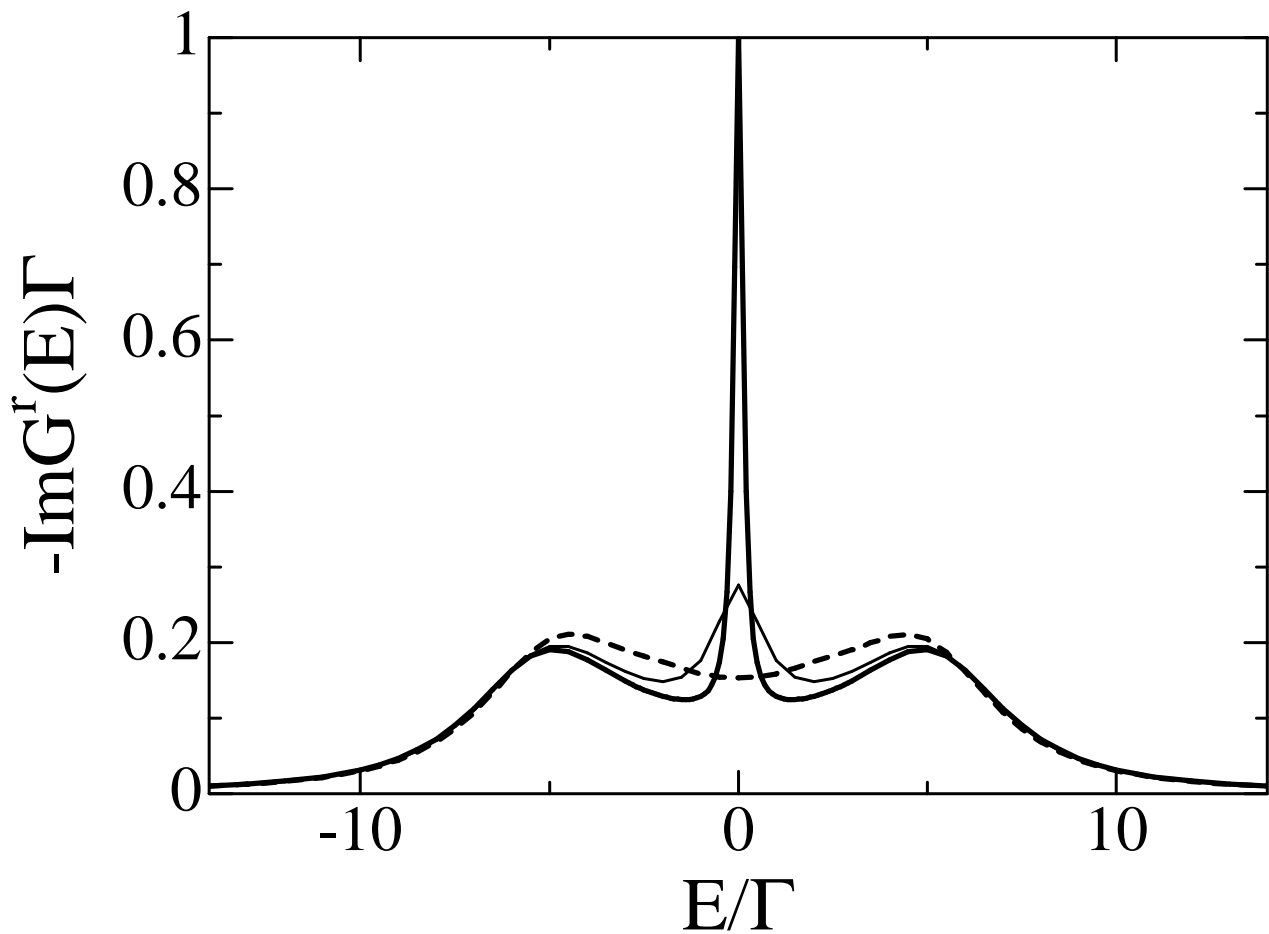


Fig.7 Hamasaki

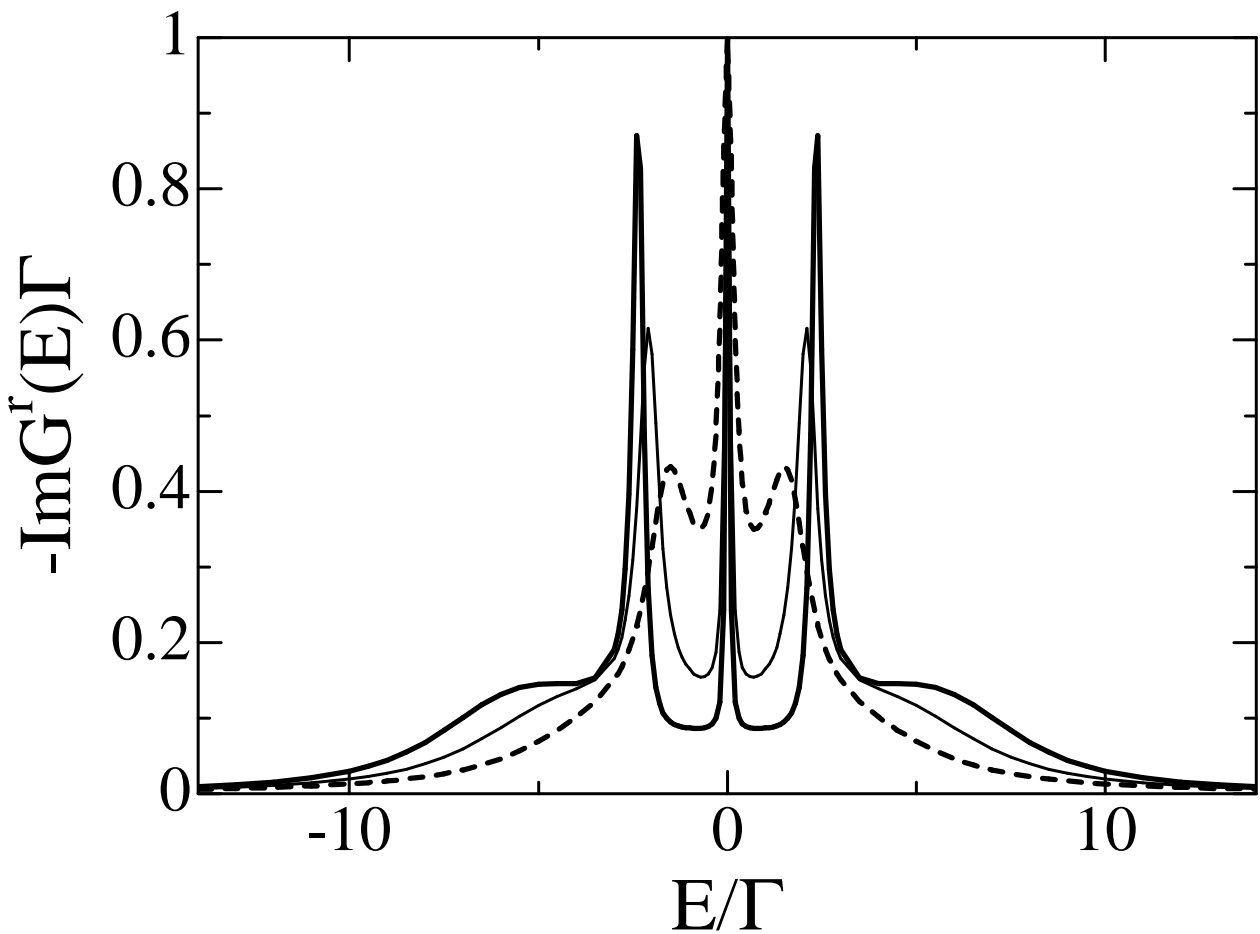


Fig.8(a) Hamasaki

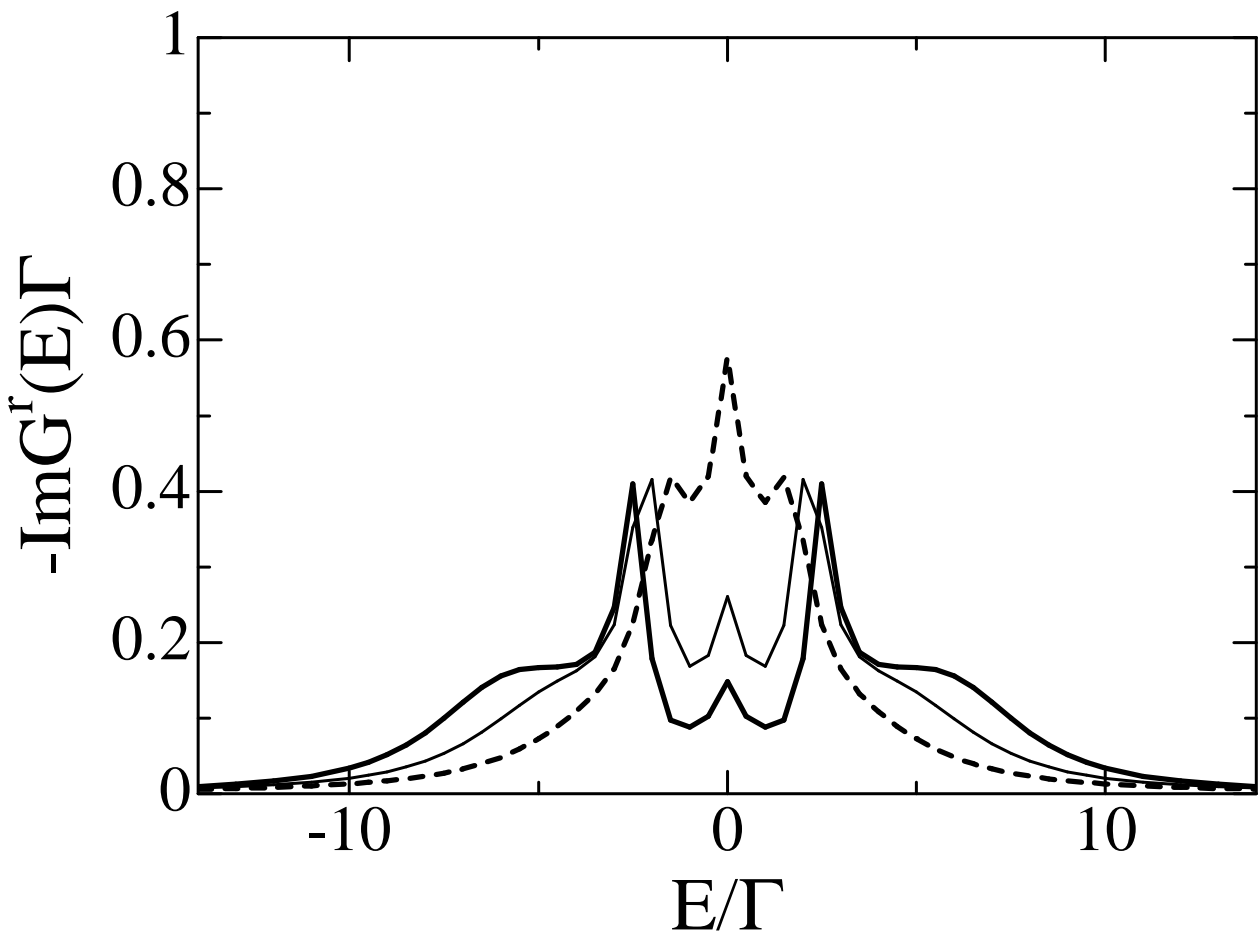


Fig.8(b) Hamasaki

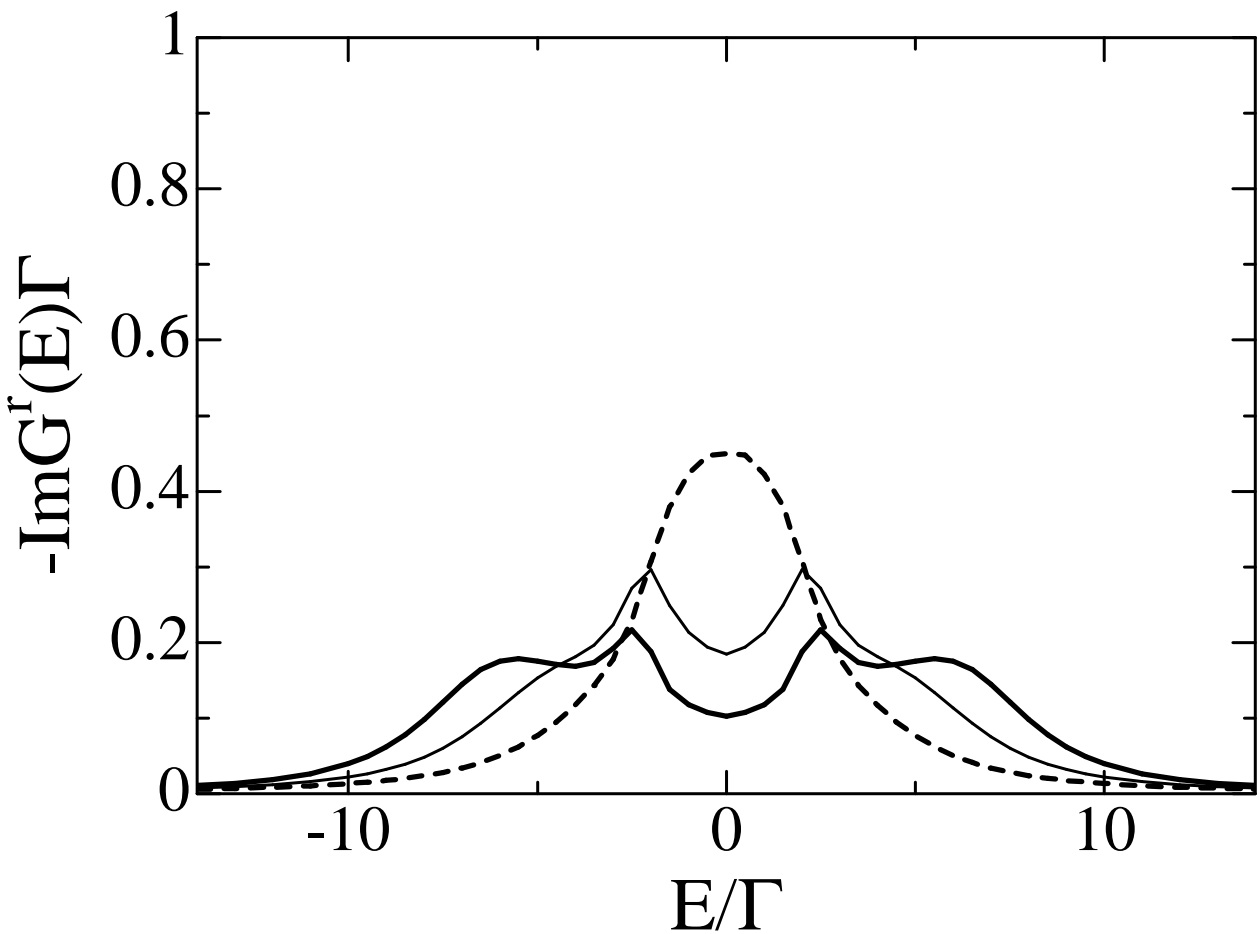


Fig.8(c) Hamasaki

